Spatiotemporal dynamics of current-density filaments in a periodically driven multilayered semiconductor device

F.-J. Niedernostheide*
Siemens AG, ZT KM 6, Otto-Hahn-Ring 6, D-81739 München, Germany

M. Kleinkes
Institut für Angewandte Physik, Universität Münster, Corrensstraße 2/4, D-48149 Münster, Germany

(Received 24 July 1998)

Results of numerical calculations of a set of reaction-diffusion equations for silicon p^+-n^+-p-n^- devices under dc and ac bias are presented. For pure dc bias, we observe self-sustained oscillations of the device voltage accompanied with pendulumlike oscillations of a current-density filament. By imposing an ac bias the device voltage shows frequency locking, quasiperiodicity, and chaos depending on the amplitude and the frequency of the ac bias. It is shown that the global oscillations are connected with corresponding frequency-locked, quasiperiodic, and chaotic filament motions. The numerical results reproduce the bifurcation sequences observed recently in experiments on multilayered silicon structures. [S0163-1829(99)00311-2]

I. INTRODUCTION

In semiconductors and semiconductor devices, diverse nonlinear mechanisms can cause a spontaneous appearance of self-sustained oscillations of, e.g., the sample current or voltage, both representing global system quantities. While in former times the interplay between an external periodic driver and the self-sustained oscillation has been studied mainly by analyzing such global quantities, recently, there has been much interest in the spatiotemporal dynamics of periodically driven semiconductors, in particular in the dynamics of electric-field domains and current-density filaments: Traveling electric-field domains under ac excitation show partly complex spatiotemporal behavior and have been intensively studied by means of numerical simulations of, e.g., two-valley models for Gunn diodes,[1,2] nonlinear transport equations for modulation-doped $GaAs/Al_xGa_{1-x}As$ heterostructures,[3] a discrete drift model for sequential resonant tunneling in superlattices,[4–6] and a drift-diffusion model for p Ge.[7] For the latter, spatially resolved measurements of the potential between the electric contacts give clear experimental evidence for the existence of different dynamical behavior including mode locking and spatially coherent as well as incoherent variations of the electric field.[8,9] Recently, also experiments in incommensurately driven superlattices have been reported.[10–12]

Concerning the dynamics of current-density filaments experimental investigations have shown that self-sustained periodic amplitude oscillations of a filament in n GaAs may transform to quasiperiodic or irregular oscillations on periodic excitations,[13,14] and numerical studies based on a one-level impact ionization model reveal that complex spatiotemporal patterns of the carrier density may appear in such periodically driven bulk semiconductors.[15] Recently, spatiotemporally resolved measurements of the recombination radiation and the potential in silicon p^+-n^+-p-n^- multilayered structures have proved that a periodic pendulumlike oscillating filament, a so-called rocking filament, reveals frequency-locked, quasiperiodic, and chaotic behavior when driven periodically.[16]

In this paper, we focus on a numerical study of a set of reaction-diffusion equations that has been derived[17] to describe the evolution and dynamical behavior of current-density filaments in the aforesaid multilayered p^+-n^+-p-n^- diodes. Adjusting the dc bias such that a rocking current-density filament is stable, the spatiotemporal dynamical behavior of the filament is investigated in dependence of the amplitude and frequency of an additional periodic ac bias imposed to the dc bias and the results are compared with experimental data.[16]

The paper is organized as follows. Section II contains a description of the physical model and the derived set of equations. The main features of the dc-biased samples are recapitulated in Sec. III. In Sec. IV, the spatiotemporal behavior is discussed for relatively small drive amplitudes. It is shown that the observed frequency-locked and quasiperiodic filament motions can be effectively evaluated by analyzing the time series of the center of the current density-filaments. These time series containing information about the local distribution of the current-density are furthermore compared with time series of the total sample current. Finally, in Sec. V we focus on filament motions that appear for sufficiently large drive amplitudes.

II. MODEL EQUATIONS

Let us first describe the model equations and recapitulate the relevant physical mechanisms the model is based on: The p^+-n^+-p-n^- device in question is considered to be composed of two parts, a p^+-n^+-p transistor and a p-n^- diode as shown in Fig. 1. Treating the transistor as avalanche transistor, which is coupled to the p-n^- diode, the following two-component set of reaction-diffusion equations can be derived[17]

$$C_e \frac{\partial V_e}{\partial t} = w\sigma_b \frac{\partial^2 V_e}{\partial x^2} - q(V_e, p), \tag{1}$$

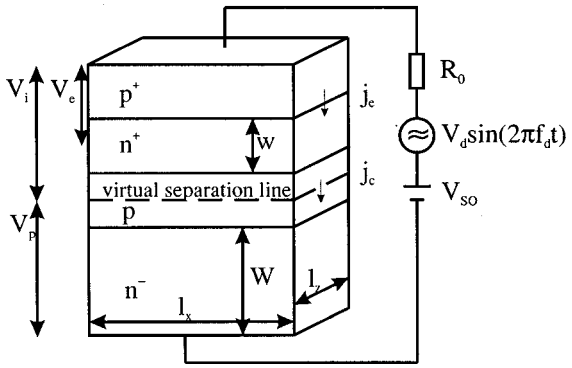

FIG. 1. Schematic sketch of the p^+-n^+-p-n^- device with electrical circuit.

$$\tau\frac{\partial p}{\partial t}=L^2\frac{\partial^2 p}{\partial x^2}+Q(V_e,p), \tag{2}$$

where V_e is the voltage drop across the p^+-n^+ emitter junction of the transistor and p denotes the average hole density in the n^- layer of the diode part. The temporal evolution of V_e is governed by the emitter capacity C_e. w and σ_b denote the width and the conductivity of the n^+ base. The temporal evolution of the mean-hole density is essentially determined by the effective lifetime τ and the diffusion length L is defined by $L^2=D_p\tau$, where D_p is the diffusion coefficient of holes in the n^- layer. The terms $q(V_e,p)$ and $Q(V_e,p)$ are determined by (for details, see Refs. 17 and 18)

$$q(V_e,p)=j_e(V_e)-j_c(V_e,p), \tag{3}$$

$$Q(V_e,p)=\frac{\tau}{eW}j_c(V_e,p)-(p-p_{no}), \tag{4}$$

with

$$j_e=j_s\left[\exp\left(\frac{V_e}{V_T}\right)-1\right]+j_r\left[\exp\left(\frac{V_e}{2V_T}\right)-1\right], \tag{5}$$

$$j_c=Mj_{sc}+\beta Mj_s\left[\exp\left(\frac{V_e}{V_T}\right)-1\right]+\frac{V_i-V_e}{\rho_L}, \tag{6}$$

$$M=\left[1-\left(\frac{V_i-V_e}{V_b}\right)^3\right]^{-1}, \tag{7}$$

where the voltage drop $V_i=V-V_p$ across the p^+-n^+-p transistor is the difference of the device voltage V and the voltage drop V_p across the p-n^- diode, which depends on the mean-hole density according to the following relation

$$V_p=V_T\ln\left(\frac{p}{p_{n0}}\right). \tag{8}$$

j_s, j_r, and j_{sc} denote the diffusion and recombination saturation current density of the p^+-n^+ junction and the saturation current density of the n^+-p junction, respectively. V_T is the thermal voltage and β the transport factor of the n^+ base. ρ_L and V_b denote the leakage resistance and the breakdown voltage of the n^+-p junction. p_{n0} is the equilibrium value of the mean-hole density, W the width of the n^- layer, and e the elementary charge.

In order to get insight into the relevant physical processes let us consider the two device parts in more detail. In usual operation under dc bias, the n^+-p junction of the p^+-n^+-p transistor is reverse biased. Suppose that the voltage drop across the n^+-p junction is sufficiently large so that charge-carrier multiplication takes place by impact ionization. Then, a small fluctuation of the emitter voltage V_e has the following consequences: Due to the essentially exponential dependence of the emitter current density on the emitter voltage, a fluctuation of V_e causes an additional injection of holes into the n^+ layer. Those holes that reach the high-field zone of the n^+-p junction generate electron-hole pairs that are separated due to the high electric field. The electrons move towards the p^+-n^+ junction and induce an additional injection of holes and, consequently, an increase of V_e. Because of this activating property of the transistor part, the variable V_e may be called an activator.

The coupling of the transistor part to the p-n^- diode results in a counteractive influence on the autocatalytic increase of V_e, because the current fluctuation caused by the fluctuation of V_e leads to an increased hole injection into the n^- layer and therefore to an augmentation of both the mean-hole concentration p in the n^- layer and the voltage drop $V_p=V_T\ln(p/p_{n0})$ across the p-n^- diode. When the device voltage V is kept constant, the voltage drop $V_i=V-V_p$ across the transistor decreases, if V_p increases. This inhibiting process in the p-n^- diode limits the autocatalytic process and, consequently, p can be viewed as an inhibiting variable.

In experiment, the device is usually connected via a load resistor R_0 to the voltage source. The device voltage V is then given by

$$V=V_s+R_0I \tag{9}$$

with

$$V_s=V_{s0}+V_d\sin(2\pi f_d t), \tag{10}$$

being the total applied voltage and consisting of the dc bias V_{s0} and the sinusoidal ac part $\tilde{V}_d(t)=V_d\sin(2\pi f_d t)$, where V_d and f_d are the drive amplitude and drive frequency. The total current I can be calculated by integrating the current-density distribution $j_c(x,t)$ along the rectangular device area $l_x\times l_z$ (cf. Fig. 1)

$$I=l_z\int_0^{l_x}j_c(x,t)dx. \tag{11}$$

Due to this relation the set of Eqs. (1) and (2) becomes a set of integro-differential equations. As outlined in detail in Ref. 18 suitable boundary conditions for the two space-dependent components V_e and p are the following

$$V_e(x=0,t)=V_{e0},\quad V_e(x=l_x,t)=V_{e0}, \tag{12}$$

$$\frac{\partial p(x=0,t)}{\partial x}=0,\quad \frac{\partial p(x=l_x,t)}{\partial x}=0. \tag{13}$$

Equations (1) and (2) have been discretized by using the finite-difference technique; in particular the Crank-Nicholson method has been applied for discretization in time. For the solution of the implicit equations resulting from the discretization of the two equations we have used a relaxation

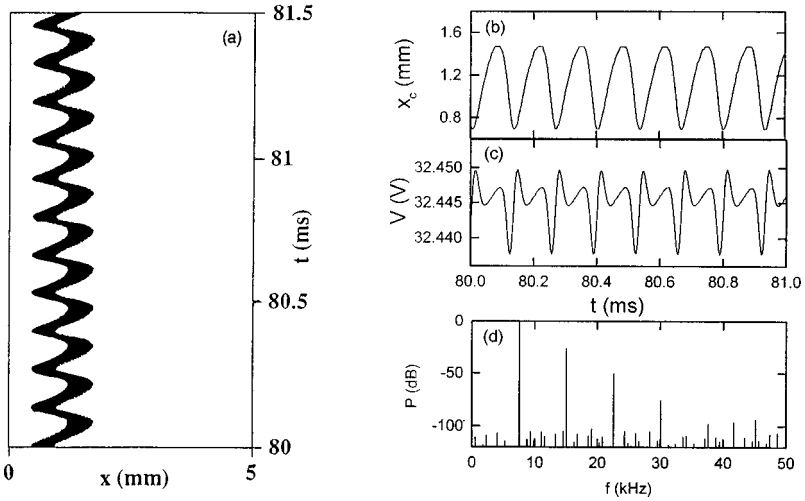

FIG. 2. Self-organized pendulumlike oscillation: Spatiotemporal distribution of j_c (a), time series $x_c(t)$ of the filament center (b), and of the device voltage $V(t)$ (c), and power spectrum P (d) of x_c. Parameters: $C_e=10^{-5}$ F/cm^2, $j_{sc}=2\times10^{-8}$ A/cm^2, $j_s=1.5\times10^{-11}$ A/cm^2, $j_r=3\times10^{-7}$ A/cm^2, $l_x=0.5$ cm, $D_p=10$ cm^2/s, $p_{n0}=10^7$ cm^{-3}, $R_0=500\ \Omega$, $T=300$ K, $V_b=42$ V, $V_{s0}=280$ V, $w=3\ \mu$m, $W=600\ \mu$m, $\beta=0.6$, $\rho_L=4\times10^4\ \Omega$ cm^2, $\sigma_b=10\ (\Omega\ \text{cm})^{-1}$, $\tau=10\ \mu$s.

method that is a simplified version of the Newton single-step method. The spatial mesh consists of 200 grid points. The third equation, Eq. (9), involving the integral term, has been solved by introducing an effective relaxation-time constant for V, which is at least two orders of magnitude faster than that of the other system variables V_e and p.

III. DC BIASED SYSTEM

Experiments[17,19] and numerical calculations[18] of Eqs. (1), (2), and (9) have shown that a static current-density filament can be stabilized in the multilayered device over a wide sample current range. When a certain sample current, typically of the order of 100–200 mA, is exceeded, the static filament bifurcates into a periodically oscillating filament that performs a pendulumlike motion around a fixed position in space. Figure 2(a) shows the time evolution of the current density j_c, which is just the current density at the interface between the two device parts, the p^+-n^+-p transistor and the p-n^- diode. The dark areas mark those parts of the distribution on which a certain threshold value, approximately 2/3 of the maximum current density, is exceeded. Thus, these regions correspond to high-current regions and mark the spatial position of the filament. In Fig. 2(b) the time series of the filament center $x_c(t)$ constructed from the temporal evolution of the complete current-density distributions is depicted. From both figures it is evident, that the filament performs a well-defined periodic pendulumlike oscillation. This is confirmed by the power spectrum of $x_c(t)$ [Fig. 2(d)] that reveals a main peak at the fundamental frequency at 7522 ± 1 Hz and harmonics of this frequency.

The filament oscillations are accompanied by oscillations of the total sample current and the device voltage, as illustrated in Fig. 2(c) for the latter one. The voltage and current oscillations have the same period as the filament oscillation, but their shapes are more complex. The reason for the obvious asymmetry lies in the influence of the Dirichlet boundary condition for V_e, which causes an alternate compression and stretching of the filament when it changes its moving direction near the boundary or in the interior of the sample. However, the filament is only weakly compressed and stretched so that the current and voltage modulations are less than 0.1% of the dc part. The shapes of the calculated voltage oscillations differ slightly from the measured ones, as the latter show only a single maximum and a single minimum during a pendulumlike oscillation period; these extrema of the voltage oscillation are connected with the two extreme filament positions. This difference between experiments and numerical results may be attributed to the fact that the chosen Dirichlet boundary condition for V_e provides only an

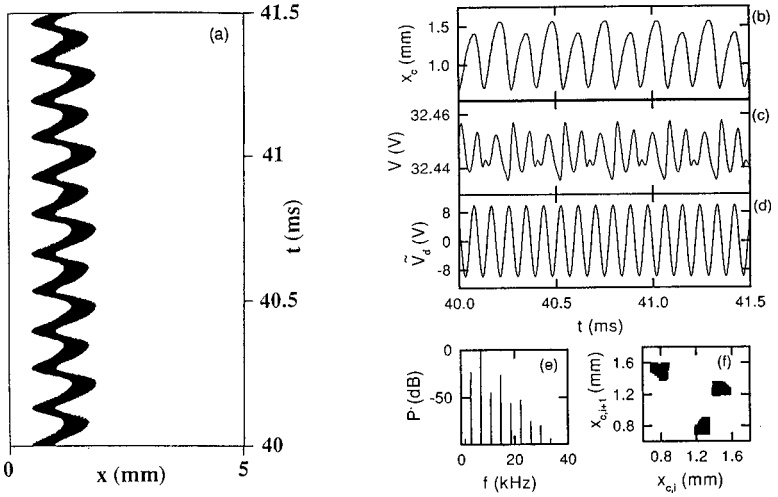

FIG. 3. Frequency-locked filament motion: Spatiotemporal distribution of j_c (a), time series $x_c(t)$ of the filament center (b), of the device voltage $V(t)$ (c), of the drive voltage (d), power spectrum (e) of x_c, and Poincaré map (f) constructed from $x_c(t)$ at a fixed phase of the drive voltage for $V_d=10$ V and $f_d=11.16$ kHz.

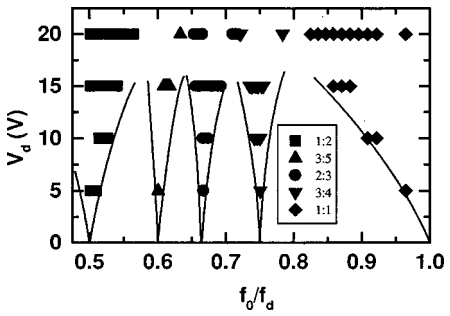

FIG. 4. Arnold tongues in the f_d-V_d control parameter space. Low-order locking ratios are marked by different symbols. The solid lines have been added to guide the eye.

approximate description of the real-boundary condition at the sample surface.

IV. FREQUENCY-LOCKED AND QUASIPERIODIC BEHAVIOR

The motion shown in Fig. 2 has been chosen as starting point for the investigations of the influence of an external periodic driving voltage on a self-organized rocking filament motion. Depending on the amplitude V_d and the frequency f_d of the ac drive voltage we find characteristic locking ratios of the filament motion and of the oscillation of the device voltage with respect to the drive voltage. An example for such a frequency-locked oscillation is shown in Fig. 3. The threshold diagram [Fig. 3(a)] reveals that the oscillating filament performs alternately a smaller and a larger elongation. This is also clearly visible in the time series $x_c(t)$ of the filament center [Fig. 3(b)]. A comparison of this time series with the drive voltage [Fig. 3(d)] yields that the filament exactly performs two fundamental oscillations during three fundamental oscillations of the driver indicating a 2:3 locking of the filament motion to the external drive. This is confirmed by the power spectrum [Fig. 3(e)] of the time series $x_c(t)$ and the Poincaré map [Fig. 3(f)] constructed by strobing $x_c(t)$ at the zero passages of the ac drive with a positive slope and plotting the $(i+1)$th vs the ith strobed value. As expected for a 2:3 locking there is only one subharmonic in the spectrum and the existence of three points in the Poincaré map is consistent with the general rule that the number of points appearing in the Poincaré map should be equal to the denominator of the locking ratio. The ac part of the device voltage $V(t)$ [Fig. 3(c)] has the same period as the filament motion and is therefore locked to the drive voltage with a 2:3 ratio, too. In the case that the drive frequency and the frequency of the spontaneous rocking oscillation are heavily detuned, frequency-locking of the filament motion is achieved by changes of the amplitude of the rocking motion as well as by variations of the velocity of the filament. This has been observed in recent experiments, likewise.[16]

The Arnold-tongue diagram (Fig. 4) shows the regions in the f_d-V_d parameter space in which the rocking filament motion is synchronized to a rational multiple of the drive frequency. Since the time series $x_c(t)$ of the filament center contains all necessary information about the spatiotemporal behavior of the filament, Lissajous figures constructed by plotting $x_c(t)$ versus the driving voltage $\tilde{V}_d$ or Poincaré section maps constructed by strobing x_c at a fixed phase of the driving voltage have been used to distinguish between synchronized and nonsynchronized filament oscillations and to determine the locking ratio. For a fixed drive amplitude the widths of the tongues order in a way that tongues with frequency ratios $(P+P')/(Q+Q')$ are smaller than those with ratios P/Q and P'/Q', as also predicted by the circle map (see, e.g., Refs. 20 and 21). With increasing drive amplitude the tongue widths increase and finally overlap leading to multistable behavior. The overlapping tongues define a critical line. In the frequency range investigated we find a critical amplitude of the driving voltage of about 14 V that corresponds to a current drive amplitude of 30 mA and is about one order of magnitude larger than that observed in experimental investigations of driven rocking filaments in multilayered devices.[16]

In between the tongues we find quasiperiodic behavior of the device voltage and of the motion of the current-density filament. Figure 5(a) shows such a quasiperiodic filament oscillation. The time series $x_c(t)$ of the filament center [Fig. 5(b)] shows no period within the calculated time interval, in which the filament and the driving voltage [Fig. 5(c)] performs several hundreds of fundamental oscillations. The appertaining power spectrum of x_c [Fig. 5(d)] clearly reveals peaks at the frequency f_0, the fundamental oscillation frequency of the self-sustained oscillation, and at the drive fre-

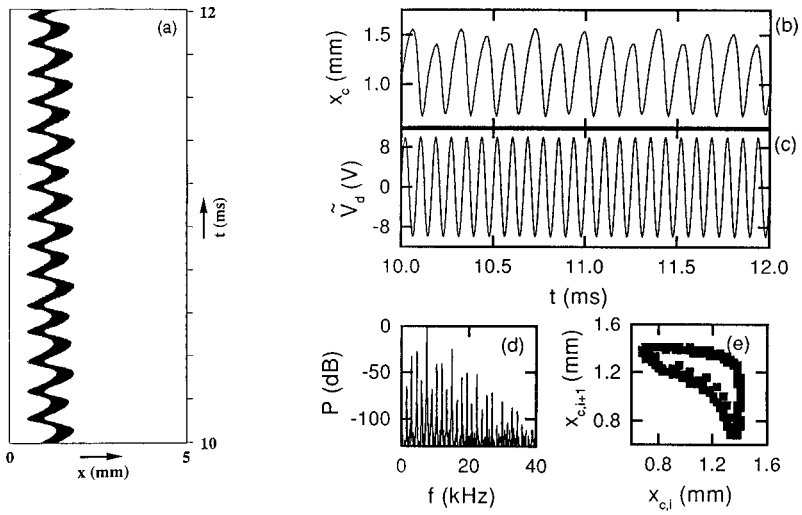

FIG. 5. Quasiperiodic filament motion: Spatiotemporal distribution of j_c (a), time series $x_c(t)$ of the filament center (b), of the drive voltage (c), power spectrum (d) of x_c, and Poincaré map (e) constructed from $x_c(t)$ at a fixed phase of the drive voltage for $V_d=10$ V and $f_d=12\,000$ Hz.

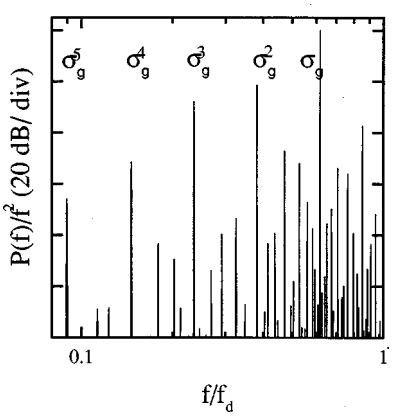

FIG. 6. Power spectrum of x_c for a quasiperiodic filament motion at the critical amplitude $V_d = 14$ V and the driving frequency f_d close to the golden mean.

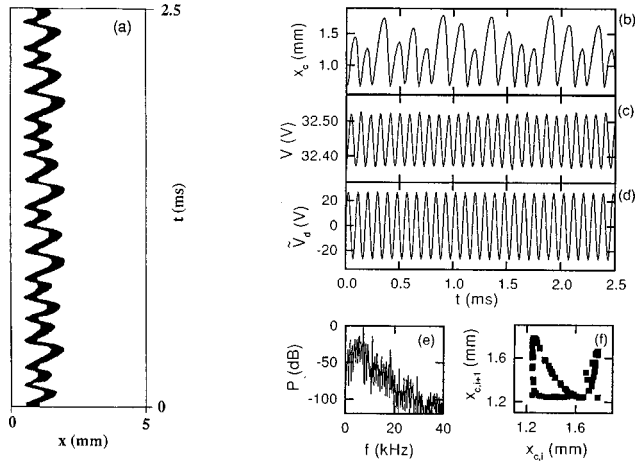

FIG. 7. Chaotic filament motion at a large drive amplitude: Spatiotemporal distribution of j_c (a), time series $x_c(t)$ of the filament center (b), of the device voltage $V(t)$ (c), of the drive voltage (d), power spectrum (e) of x_c, and return map (f) constructed from successive maxima of $x_c(t)$ for $V_d = 27$ V and $f_d = 10980$ Hz.

quency f_d. Peaks appear also at frequencies $f = nf_0 + mf_d$, where n and m are whole numbers. A further indication for the quasiperiodic filament oscillation is given by the Poincaré section map [Fig. 5(e)], which is forming an approximately closed curve, giving evidence of a dense covering of the toroidal attractor.

On the experimental side[16] a corresponding quasiperiodic rocking filament oscillation has been proved by measuring the potential on the sample surface between the electrodes. It turned out that the local potential, measured on a line parallel to the contacts in a region where the filament oscillation takes place, is quasiperiodic at any position covered by the moving filament. A comparison of the local potential with the global device voltage oscillation revealed that the two signals are in phase when the local potential is measured at the turning point near the sample boundary, while the potential near the interior turning point and the device voltage oscillate in antiphase. Along the line between the turning points the phase shift increases continuously from zero to 180°; the same behavior can be found in numerical calculations for the temporal evolution of the potential distribution V_p across the p-n^- junction.

V. UNIVERSAL BEHAVIOR AND CHAOTIC MOTIONS

When the drive amplitude is adjusted to the critical value and the ratio of the self-sustained frequency to the drive frequency is equal to the golden mean $\sigma_g = (\sqrt{5}-1)/2$, the circle map predicts a universal form for the low-frequency power spectrum of its dynamic variable (see, e.g., Ref. 22). By analyzing *global* quantities as the total sample current such a universal form of the power spectrum has been found experimentally for sinusoidally driven p-Ge in excellent agreement with the circle map.[23] As the main aim of our paper is to investigate the influence of an external periodic excitation on the spatiotemporal behavior of the current-density filament, we focus again on an analysis of x_c in order to check whether such universal laws are also valid for the *local* filament motion.

Figure 6 shows the spectrum of x_c for a drive amplitude $V_d = 14$ V, our best approximation to the critical amplitude at the golden mean. The distinctive main peaks in the spectrum, which is normalized to f^2, occur at frequency ratios $f/f_d = \sigma_g^n$, where n is a whole number. These first-generation peaks are visible up to the ninth power (not shown here). Peaks with higher n values appear, when the filament motion is traced for a longer time interval. Inside the frequency intervals $[\sigma_g^n, \sigma_g^{n+1}]$ a characteristic peak order is visible. All relevant peaks in these frequency intervals are in correspondence to the respective peaks of the self-similar spectrum predicted by the circle map. A fully developed self-similar spectrum of the quasiperiodic filament motion is expected to appear in the low-frequency limit, that demands again to trace the filament motion for a longer time interval with a finer spatial discretization and a precise adjustment of the driving ratio to the golden mean.

For amplitudes of the driving voltage larger than those defined by the critical line at which the tongues start to overlap, the time series of the filament center show period-doubling routes and transitions to chaotic motions inside the tongues. An example of a chaotic motion is shown in Fig. 7. Chaos is indicated by the shape of the return map, that has been constructed by using successive local maxima of the time series of the filament center, as well as by the increasing broad-band noise in the associated power spectrum. Note that due to the small deformations the filament suffers during the motion, the chaotic behavior is also visible in the time series of the device voltage, however much less pronounced than in the filament motion itself. Furthermore, for large driving amplitudes the actual filament motion depends on the initial conditions and the way of parameter changing indicating multistability, as also predicted by the circle map.

VI. CONCLUDING REMARKS

In conclusion, we point out that the numerical results presented in this paper reproduce the essential features of ac driven rocking filaments found in recent experiments: Beyond frequency-locked and quasiperiodic rocking filament motions also period doublings and chaotic motions of rocking filaments may evolve, depending on the amplitude and frequency of the driver. In particular, frequency locking is

achieved in that both the amplitude and the duration of the fundamental rocking oscillation are adapted to the external drive. The frequency-locked states order in the form of Arnold tongues in the V_d-f_d parameter space, and irregular filament motions, which appear inside the tongues for sufficiently large driving amplitudes, are temporally chaotic but spatially coherent filament motions. This shows that the external driver influences mainly the rocking mode, while there is only a very weak interaction with other possible fundamental oscillation modes, as amplitude or width oscillations. Consequently, the time series of the filament center reflects the main features of the low-dimensional filament dynamic and shows universal behavior in agreement with the predictions of the circle map as has been illustrated for the quasiperiodic filament motion with a drive ratio close to the golden mean.

ACKNOWLEDGMENT

The authors would like to acknowledge the financial support of the Deutsche Forschungsgemeinschaft.

*On leave from Institut für Angewandte Physik, Universität Münster, Corrensstraße 2/4, D-48149 Münster, Germany.

[1] E. Mosekilde, R. Feldberg, C. Knudsen, and M. Hindsholm, Phys. Rev. B **41**, 2298 (1990).
[2] E. Mosekilde, J. S. Thomson, C. Knudsen, and R. Feldberg, Physica D **66**, 143 (1993).
[3] R. Döttling and E. Schöll, Solid-State Electron. **37**, 685 (1994).
[4] O. M. Bulashenko and L. L. Bonilla, Phys. Rev. B **52**, 7849 (1995).
[5] O. M. Bulashenko, M. J. García, and L. L. Bonilla, Phys. Rev. B **53**, 10 008 (1996).
[6] L. L. Bonilla, O. M. Bulashenko, J. Galán, M. Kindelan, and M. Moscoso, Solid-State Electron. **40**, 161 (1996).
[7] M. J. Bergmann, S. W. Teitsworth, L. L. Bonilla, and I. R. Cantalapiedra, Phys. Rev. B **53**, 1327 (1996).
[8] A. M. Kahn, D. J. Mar, and R. M. Westervelt, Phys. Rev. Lett. **68**, 369 (1992).
[9] A. M. Kahn, D. J. Mar, and R. M. Westervelt, Phys. Rev. B **46**, 7469 (1992).
[10] Y. Z. Zhang, R. Klann, K. H. Ploog, and H. Grahn, Appl. Phys. Lett. **69**, 1116 (1996).
[11] Y. Z. Zhang, J. Kastrup, R. Klann, K. H. Ploog, and H. T. Grahn, Phys. Rev. Lett. **77**, 3001 (1996).
[12] K. J. Luo, H. T. Grahn, K. H. Ploog, and L. L. Bonilla, Phys. Rev. Lett. **81**, 1290 (1998).
[13] K. Aoki, K. Yamamoto, and N. Mugibayashi, J. Phys. Soc. Jpn. **26**, 26 (1988).
[14] J. Spangler and W. Prettl, Phys. Scr. **T55**, 25 (1994).
[15] K. Aoki, Int. J. Bifurcation Chaos Appl. Sci. Eng. **7**, 1059 (1997).
[16] F.-J. Niedernostheide, C. Brillert, B. Kukuk, H.-G. Purwins, and H.-J. Schulze, Phys. Rev. B **54**, 14 012 (1996).
[17] F.-J. Niedernostheide, B. S. Kerner, and H.-G. Purwins, Phys. Rev. B **46**, 7559 (1992).
[18] F.-J. Niedernostheide, M. Ardes, M. Or-Guil, and H.-G. Purwins, Phys. Rev. B **49**, 7370 (1994).
[19] F.-J. Niedernostheide, A. Arps, R. Dohmen, H. Willebrand, and H.-G. Purwins, Phys. Status Solidi B **172**, 249 (1992).
[20] M. J. Feigenbaum, L. P. Kadanoff, and S. J. Shenker, Physica D **5**, 370 (1982).
[21] S. J. Shenkder, Physica D **5**, 405 (1982).
[22] S. Ostlund, D. Rand, J. Sethna, and E. Siggia, Physica D **8**, 303 (1983).
[23] E. G. Gwinn and R. M. Westervelt, Phys. Rev. Lett. **57**, 1060 (1986); **59**, 247(E) (1987).